Review Article

Formulation and Characterization of Rosin-Based Bioresins Modified with Palm Wax, Microwax, and Olein for Sustainable Biocomposite Applications

Siti Agustina, Fajriyan and Lukman Junaidi
Research Center for Sustainable Industrial and Manufacturing Systems, National Research and Innovation Agency (BRIN), Tangerang Selatan, Banten, Indonesia

Aton Yulianto, Wiwik Handayani, Eddy Sapto Hartanto, Karnadi* and Budiyanto
Research Center for Process Technology, National Research and Innovation Agency (BRIN), Tangerang Selatan, Banten, Indonesia

Ahmad Suhendra
Research Center for Fuel Technology, National Research and Innovation Agency (BRIN), Tangerang Selatan, Banten, Indonesia

Ade Saepudin and Ahmad Kamil
Research Center for Behavioral and Circular Economics, National Research and Innovation Agency (BRIN), Jakarta, Indonesia

Firdha Aulya Syamani
Research Center for Bioproduct and Biomass National Research and Innovation Agency-Indonesia, Cibinong, Jawa Barat, Indonesia

* Corresponding author. E-mail: karn002@brin.go.id DOI: 10.14416/j.asep.2026.04.010
Received: 8 October 2025; Revised: 15 November 2025; Accepted: 3 February 2026; Published online: 28 April 2026

Abstract
The formulation of sustainable bioresins sourced from renewable materials generates considerable opportunities for biocomposite uses in sectors such as food, packaging, and cosmetics. This research focused on the formulation and characterization of rosin-based bioresins that were modified with palm wax, microwax, and olein at various concentrations (5%, 10%, and 15%). The bioresins were formulated by melting rosin and subsequently adding additives, followed by casting and cooling processes. The analysis using Fourier-transform infrared spectroscopy (FTIR) verified the presence of functional groups associated with the resin's esterification and the addition of additives. The assessment of thermal stability was performed using thermogravimetric analysis (TGA) and differential scanning calorimetry (DSC), which indicated distinct degradation phases that were affected by the type and concentration of the additives. DSC revealed distinct melting temperatures (Tm) ranging from 40 to 90 °C and glass transition temperatures (Tg) from 60 to 230 °C. TGA showed degradation onset temperatures (Td) between 370 and 410 °C, indicating excellent thermal stability across all formulations. Hardness testing demonstrated composition-dependent mechanical reinforcement, with B-series and C-series presenting improved resistance compared to A-series. The combined thermal–mechanical evaluation demonstrates that bioresin B provides the most balanced performance due to synergistic contributions of microcrystalline wax, yielding improved hardness (13.12 ± 10.43 kg in B_2) while maintaining high thermal stability (Td = 390 °C). These findings highlight the potential of modified bioresins as sustainable alternatives with tunable structure–property relationships suited for packaging films, protective coatings, and solid cosmetic matrices. Thermal analysis indicated enhanced stability in systems modified with palm wax and microwax, while olein contributed to an increase in flexibility at the expense of thermal resistance. Overall, modified bioresin B emerged as the optimal formulation for structural and packaging applications due to its superior thermal stability, increased hardness, and enhanced molecular interactions.

Keywords: Biocomposites, Biorefinery, Hardness, Palm wax, Rosin-based bioresin, Thermal analysis

1 Introduction

The growing environmental issues and the diminishing petroleum resources have heightened the exploration of renewable and biodegradable materials for composite applications. The rising need for sustainable and renewable materials in industrial sectors has promoted research into natural resin–based systems as substitutes for petroleum–derived polymers.

Biobased resins sourced from natural feedstocks like rosin and vegetable waxes have emerged as viable alternatives to synthetic resins due to their sustainability, low toxicity, and biodegradability [1]. Rosin (*Resina colophonium*), a natural resin extracted from pine trees, shows good film–forming capabilities, tackiness, hydrophobicity, and compatibility with various additives, rendering it a promising candidate for bioresin production. Its structure, characterized by abietic–type resin acids, offers reactive sites for chemical modification, making it appropriate for use in biocomposites and functional coatings [2].

Additionally, rosin is plentiful, cost–effective, and biodegradable, establishing it as an ideal substitute for synthetic polymers across diverse applications [3]. Prior research has shown its compatibility with both natural and synthetic polymers, facilitating customized property modifications [4]. These characteristics make rosin an attractive base for biocomposites, where it can function as a matrix material for natural fiber reinforcements. Rosin is primarily made up of resin acids containing carboxylic functional groups [5]. These functional groups provide reactivity and adhesion characteristics that are beneficial for resin matrices within composite systems. Nevertheless, pure rosin is characterized by brittleness, low thermal stability, and restricted flexibility, which limit its direct application in advanced material systems such as biocomposites [6], [7].

To address these limitations, modifiers such as palm wax, microwax, and olein were selected for this study. Recent advancements have focused on improving the functional and mechanical characteristics of bioresins through chemical modification and blending with bio–based or inorganic fillers to produce high–performance biocomposites [8].

Palm wax, a vegetable–derived wax, possesses advantageous attributes such as biodegradability and hydrophobicity. Palm wax is a triglyceride–based material with high crystallinity, contributing to enhanced hardness and hydrophobicity when incorporated into resin systems [9]. Microwax (microcrystalline wax) enhances toughness and structural integrity, while olein, a liquid component of palm oil, improves plasticity and diminishes brittleness [10]–[12]. Microwax, composed mainly of long–chain hydrocarbons, introduces thermal stability and improves moisture resistance in bioresin blends [13]. These wax additives modify the resin's polarity, crystallinity, and mechanical properties, enabling its application as a renewable composite matrix [14].

These modifications are aligned with the growing need for eco–friendly materials in food packaging, cosmetic formulations, and biomedical coatings [15]. The combination of these modifiers aims to create tailored bioresins with tunable mechanical and thermal properties for various applications, including food packaging, cosmetics, and biomedical uses such as wound dressings and controlled–release drug delivery systems [16], [17].

Spectroscopic and thermal characterization methods such as Fourier–Transform Infrared Spectroscopy (FTIR), Thermogravimetric Analysis (TGA), and Differential Scanning Calorimetry (DSC) are essential for understanding the chemical interactions and thermal behavior of modified bioresins. FTIR analysis is capable of confirming the functional groups linked to rosin and its derivatives, whereas TGA and DSC offer valuable insights into thermal degradation and stability when subjected to heating conditions [18]. Furthermore, mechanical properties, particularly hardness, are critical for determining the applicability of bioresins in load–bearing or structural composite systems [19].

Recent developments indicate that wax–modified bioresins can function as matrices for biocomposites incorporating natural fibers, achieving an optimal balance between mechanical strength and biodegradability [20]. However, systematic studies comparing different modifier combinations (palm wax, microwax, olein) and their effect on chemical structure, thermal stability, and mechanical performance remain limited.

Despite the potential of rosin–based materials, comprehensive studies on multi–component modification using natural waxes and olein remain limited, particularly in terms of their thermal, mechanical, and functional characteristics for multi–sector applications. Most previous research focuses on rosin as an additive rather than a primary matrix for bioresin systems [21]. Recent research has intensified efforts to improve the performance of bio–based resin systems through functional modification using natural

waxes, triglycerides, and rosin derivatives. Rosin–derived epoxy thermosets possess high rigidity and elevated Tg, but their intrinsic brittleness necessitates flexible modifiers to widen their application [22].

Natural wax modifiers have also been used to tune melting behavior and crystalline structures. Palm–based waxes increase crystallinity, raise the melting point, and improve barrier strength in biodegradable films [23]. Triglyceride–based plasticizers, such as olein, introduce an opposite effect. Olein lowers Tg, increases molecular mobility, and improves ductility in bioresin matrices [24]. Olein–derived plasticizers improve spreadability and reduce brittleness in natural resin coatings [25]. These findings underline that olein acts primarily as a plasticizing agent but can also enhance cohesive interactions when present at moderate levels. A limited number of works have simultaneously evaluated thermal and mechanical parameters. DSC, TGA, and hardness can be integrated to reveal structure–property relationships in bioresin composites, showing strong correlations between Tg, crystal domain formation, and mechanical strength [26].

Despite these advancements, no study to date has systematically compared the combined effects of palm wax, microcrystalline wax, and olein within a single rosin–based bioresin platform, nor linked DSC/TGA transitions to hardness behavior across multiple formulations. The present work fills this gap by providing a comparative structure–property assessment of nine modified bioresins (A_1–C_3), establishing clear correlations between crystalline modifiers (palm wax, microcrystalline wax), mobility–enhancing modifiers (olein), and resulting thermal–mechanical properties.

The novelty of this research includes: 1) It presents the first comparative evaluation of palm–wax, microcrystalline–wax, and olein–modified rosin bioresins. 2) It integrates thermal–mechanical correlation analysis. 3) It establishes a structure–property framework for natural-wax bioresins, enabling future materials design.

This study aims to develop rosin–based bioresins modified with palm wax, microwax, and olein and to evaluate their physicochemical, thermal, and mechanical characteristics. The findings are expected to highlight the potential of these modified bioresins as sustainable biocomposite applications, including food coatings, packaging, cosmetics, and biomedical materials. While rosin and individual modifiers have been studied, a systematic comparative study of the effects of palm wax, microwax, olein, and their hybrids on the thermo–mechanical properties of rosin–based bioresins is lacking [27]–[29].

2 Material and Methods

2.1 *Materials*

Rosin was purchased from Perhutani Fine Chemical in Pemalang, Indonesia. Its specifications indicate that it is solid, yellow, with a melting point that varies between 70 °C and 90 °C. Palm wax grade SM 2000 was purchased from PT Mega Surya Mas in Indonesia. The specifications include FFA = 0.077%, IV (Titration) = 0.14, and a melting point of 59 °C. Olein was obtained from PT Bimoli in Indonesia, with specifications of FFA at 0.1%, an iodine number of 56, a melting point of 24 °C, and a cloud point of 10 °C. Microwax, which has a melting point of 60 °C, was purchased from a local market in Jakarta, Indonesia.

2.2 *Preparation of modified bioresin*

In this study, 3 types of modified bioresin products were prepared, namely modified bioresin A, B, and C. Modified bioresin A (rosin + palm wax) was prepared by heating rosin until completely liquefied, and palm wax was added at concentrations of 5%, 10%, and 15%. The mixture was stirred at 500 rpm and a temperature of 150 °C for a period of 30 min. Modified bioresin B (rosin + palm wax + microwax) was prepared by heating the rosin until completely liquefied, then palm wax and microwax were added in total concentrations of 5%, 10%, and 15% (w/w). The ratio of palm wax and microwax was 1: 1. The mixture was stirred at 500 rpm for 30 minutes at 150 °C. Modified bioresin C (rosin + olein) was prepared by heating rosin until completely liquefied, and olein was added at 5%, 10%, and 15% (w/w). The mixture was stirred at 500 rpm and a temperature of 150 °C for 30 minutes. Subsequently, each modified bioresin A, B, and C was cast into molds and cooled at 25 °C for 3 h.

2.3 *Testing of modified bioresin characteristics*

2.3.1 Fourier transform infrared spectroscopy

FTIR was employed to monitor the chemical transformations occurring during the synthesis of the additives and the intermediate reaction products. A Shimadzu IR–Prestige–21 instrument was utilized with 4 cm^{-1} resolution, across a wavenumber range of 400 to 4000 cm^{-1}.

2.3.2 Thermal analysis

Thermogravimetric analysis

The thermal stability of the modified bioresin was evaluated utilizing the TGA Q–50 from TA Instruments (USA). About 15.0 mg of the samples were positioned in an aluminum pan and subsequently exposed to a synthetic air atmosphere (40 mL/min) ranging from 25 to 700 °C, with a heating rate of 10 °C/min.

Differential scanning calorimetry (DSC)

The thermal transitions of the modified bioresin were examined using a DSC–50 from TA Instruments (USA). About 10.0 mg of the samples were enclosed in a DSC pan and then cooled from 50 °C to 25 °C before being heated to 200 °C. The cooling and heating rates were performed at 10 ºC/min in a nitrogen atmosphere (40 mL/min).

2.3.3 Hardness test

The hardness of the modified bioresins was evaluated by a needle penetration method, adapted from ASTM D1321 [30] and AOAC Official Method 965.47 [31]. The sample was prepared by filling modified bioresin into a cylindrical mold that has a thickness of 6 mm and a diameter of 10 mm. In this analysis, the standard instruments were utilized. A 1 mm needle under a 300 g load was allowed to penetrate the sample surface for 5 ± 0.1 seconds at 20 ± 2 °C. The penetration depth (mm) was recorded using an electronic caliper; four measurements were taken around the circumference, and one measurement was conducted at the center of the specimen. The mean of five replicates was calculated for each sample. This test quantifies the penetrative resistance, which is inversely proportional to material softness.

3 Result and Discussion

3.1 3.1 *Chemical structure*

FTIR spectroscopy was utilized to examine the structural characteristics and chemical interactions in the modified bioresins. The spectra for modified bioresin A, B, and C are shown in Figures 1–3, respectively. Each spectrum revealed the presence of functional groups corresponding to rosin–based matrices and their modifications with palm wax, microwax, and olein.

3.1.1 The FTIR analysis of modified bioresin A

The FTIR spectrum for modified bioresin A (Figure 1) illustrates the spectra of modified bioresin A_1 (rosin and 5% palm wax), modified bioresin A_2 (rosin and 10% palm wax), and modified bioresin A_3 (rosin and 15% palm wax). The FTIR spectrum revealed characteristic absorption peaks corresponding to both rosin and palm wax components. The incorporation of palm wax into rosin alters both the hydrogen bonding network and the hydrophobic profile of the material.

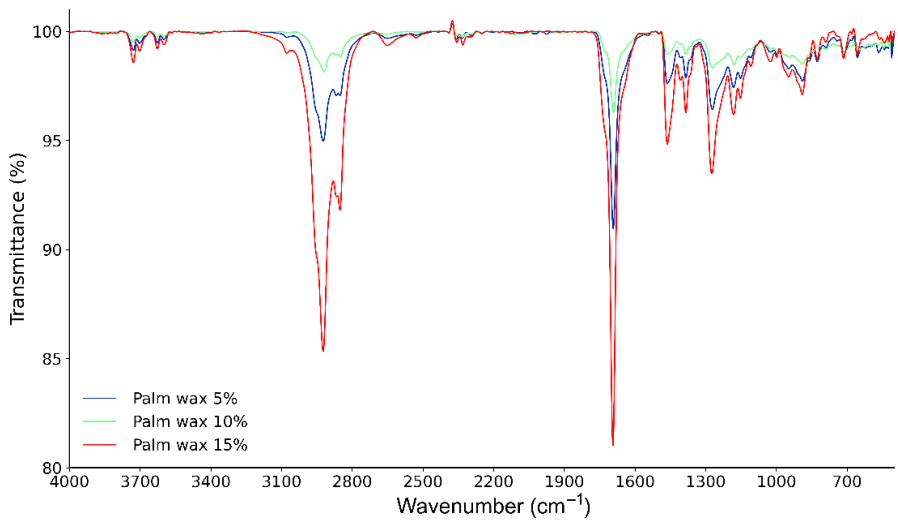

Figure 1: The FTIR spectrum of modified bioresin A.

The FTIR spectrum of A_1 preserved the main bands of rosin: the broad O–H stretching at ~3440 cm^{-1}, the C=O stretching at ~1690 cm^{-1} (abietic acid derivatives), and C–H stretching at 2924/2853 cm^{-1}. With 5% palm wax addition, slight intensification of the aliphatic C–H bands and the appearance of a weak ester C–O stretch at 1170 cm^{-1} indicated the incorporation of wax esters [32]. This suggests that palm wax begins to act as a plasticizer, weakening hydrogen bonding and increasing hydrophobicity [33].

The FTIR spectrum of A_2 displayed stronger modifications. The intensity of the O–H stretching band decreased, indicating disruption in the intermolecular hydrogen bonding network of rosin. The C=O band shifted slightly (to approximately 1686 cm^{-1}), consistent with ester–carboxyl interactions between palm wax and rosin [34]. The aliphatic C–H stretching bands (2920 and 2850 cm^{-1}) intensified further, reflecting an increase in hydrophobic reinforcement. This concentration represents an optimal miscibility point, resulting in a balanced hydrogen–bond reduction and hydrophobic enhancement.

The FTIR spectrum of A_3, at higher palm wax loading, wax–related peaks dominated the FTIR spectrum. The C–H bands at 2916 and 2850 cm^{-1} became the most prominent features. The O–H stretching band nearly disappeared, indicating a substantial decrease in hydrogen bonding, while the C=O band broadened due to heterogeneous chemical environments [35]. The stronger C–O band at ~1170 cm^{-1} confirmed significant ester content. These characteristics indicate over–plasticization, consistent with a more amorphous structure and weaker rigidity, consistent with DSC–TGA findings.

The FTIR results show a progressive chemical shift from rosin–dominant to wax–dominant structures as palm wax content increases. Modified bioresin A_1 shows minimal modifications and initial hydrophobic reinforcement. Modified bioresin A_2, indicates a strong ester–carboxyl interaction, optimal miscibility, and improved flexibility without major loss of structural integrity. Modified bioresin A_3 exhibits characteristics such as over–plasticization, a predominance of aliphatic wax features, diminished hydrogen bonding, and heterogeneity. Together with thermal data, the FTIR spectra confirm that modified bioresin A_2 provides the most balanced composition for sustainable bioresin applications in food coatings, packaging, and cosmetics.

The addition of palm wax results in higher crystallinity within the modified bioresin matrix due to its saturated hydrocarbon chains, as indicated by the sharper intensity of CH stretching peaks. This modification contributes to improved flexibility and reduced brittleness, addressing a significant limitation of pure rosin bioresin [36], [37]. The enhanced structural network is expected to improve dimensional stability under varying environmental conditions, making this formulation suitable for rigid biocomposites and food packaging applications that require durability and moisture resistance [38].

Overall, the FTIR spectra confirm that modified bioresin A retains both polar functional groups (O–H and C=O) and elongated aliphatic chains. This dual functionality is beneficial for biocomposite applications. Polar groups enable hydrogen bonding or dipole–dipole interactions with hydroxyl–rich lignocellulosic fibers, thereby enhancing interfacial adhesion, while hydrophobic hydrocarbon segments contribute to improved water resistance and dimensional stability [39].

3.1.2 The FTIR spectrum of modified bioresin B

The FTIR spectrum of modified bioresin B (Figure 2) illustrates the spectra of modified bioresin B_1 (rosin and 5% palm wax + microwax), B_2 (rosin and 10% palm wax + microwax), and B_3 (rosin and 15% palm wax + microwax).

The FTIR spectrum of modified bioresin B_1 retained the characteristic rosin bands: a broad O–H stretching around 3440 cm^{-1}, a sharp C=O stretching associated with carboxylic acids near 1690 cm^{-1}, and aromatic C=C stretching close to 1600 cm^{-1}. With 5% wax blend, an intensification of aliphatic C–H stretching bands at 2922/2850 cm^{-1} was observed, consistent with hydrocarbon enrichment. A weak band at approximately 720 cm^{-1} emerged, which is characteristic of long–chain, $–(CH_2)_n–$ rocking modes, found in waxes [40]. This suggests the beginning of molecular dispersion of wax esters within the rosin matrix.

In modified bioresin B_2, the O–H stretching intensity declined, reflecting hydrogen–bond disruption. The C=O stretching band exhibited a slight shift to approximately 1686 cm^{-1}, which suggests the presence of ester–carboxyl interactions between wax esters and the abietic acid derivatives of rosin [18]. The peaks associated with C–H stretching became more pronounced and sharper, while the ester C–O stretching at around 1170 cm^{-1} showed an increase in

intensity compared to modified bioresin B_1. This observation confirms improved compatibility and stronger physical interactions. Existing literature on wax–resin blends supports such band shifts as indicators of miscibility and the reinforcement of ester–hydrocarbon interactions [41].

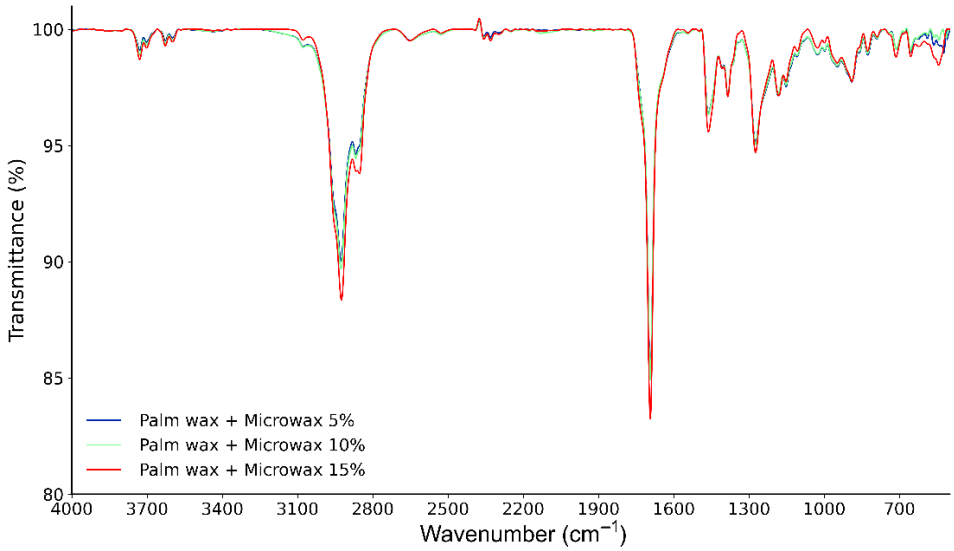

Figure 2: The FTIR spectrum of modified bioresin B.

In the case of modified bioresin B_3, which had a higher wax loading, the FTIR spectrum was predominantly characterized by features of wax. The aliphatic C–H stretching bands at 2916 and 2850 cm^{-1} became the most significant, effectively overshadowing the polar functionalities of rosin. The O–H stretching band diminished considerably, while the C=O band exhibited broadening and a slight downfield shift, indicative of heterogeneous environments resulting from phase segregation [42].

The FTIR results demonstrate a clear progressive structural transition. Modified bioresin B_1, retains rosin's identity, with initial hydrocarbon reinforcement. Modified bioresin B_2 exhibits a balanced interaction between ester and carboxyl groups, ensuring optimal miscibility and enhanced flexibility without any phase separation. Modified bioresin B_3 is characterized by dominant wax features, a reduction in hydrogen bonding, and indications of heterogeneity and over–plasticization. The data obtained from DSC–TGA analyses confirm that modified bioresin B_2 represents the most balanced formulation regarding its structural integrity and potential performance, whereas bioresin B_3 tends to exhibit wax–dominant characteristics.

This hybrid composition results in greater hardness and improved thermal stability compared to single–modifier formulations, as confirmed by thermal analysis. The dense structural network formed by palm wax and microwax significantly improves the rigidity and mechanical strength of the resin, rendering it suitable for applications in rigid packaging materials, durable coatings, and structural containers for cosmetics [43]. These properties are particularly beneficial for scenarios where maintaining shape and thermal resilience is essential. The integration of rosin (which provides polar interactions), palm wax (rich in ester–based triglycerides), and microwax (composed of non–polar long–chain hydrocarbons) results in a composite matrix that effectively balances polarity and hydrophobicity. This amphiphilic character is beneficial in biocomposite systems because polar groups support fiber adhesion, while the hydrocarbon components enhance moisture resistance and overall processability [44].

3.1.3 The FTIR spectrum of Modified Bioresin C

The FTIR spectrum of modified bioresin C (Figure 3) illustrates the spectra of modified bioresin C_1 (rosin and 5% olein), C_2 (rosin and 10% olein), and C_3 (rosin and 15% olein).

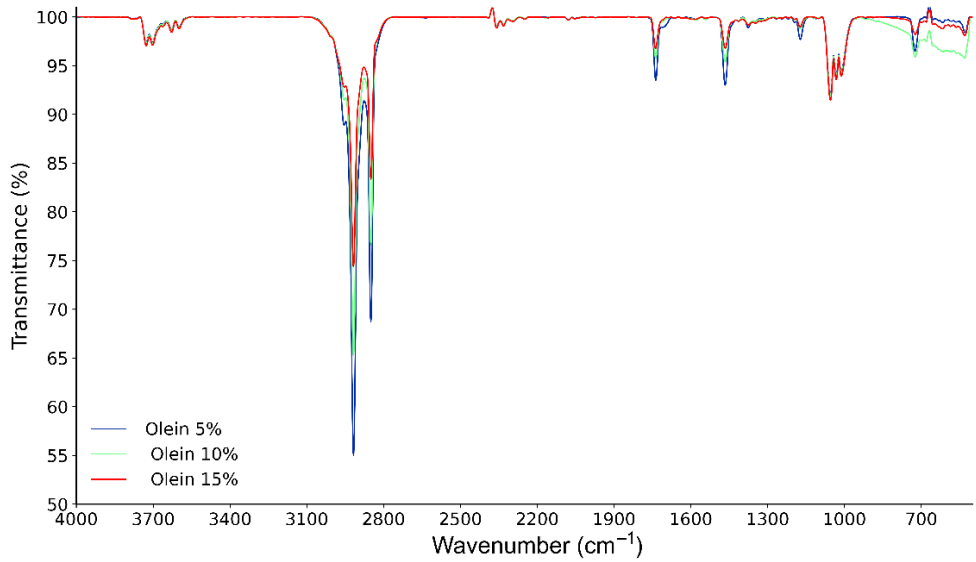

Figure 3: The FTIR spectrum of modified bioresin C.

The spectrum of modified bioresin C_1 shows the unique O–H stretching (~3440 cm^{-1}), C=O stretching (around 1690 cm^{-1}), and C=C stretching (around 1600 cm^{-1}) that are typical of rosin. When 5% olein is added, there's a slight boost in the aliphatic C–H stretching bands at 2924/2853 cm^{-1}, which indicates the inclusion of hydrocarbon chains. Moreover, a faint band appears around 1743 cm^{-1}, linked to the ester C=O of olein triglycerides [3]. This indicates an initial blending of molecules without much phase separation.

In modified Bioresin C_2, there are some significant changes in the spectrum. The intensity of the O–H band (around 3440 cm^{-1}) decreases, indicating a reduction in hydrogen bonding. The ester C=O band (around 1743 cm^{-1}) becomes more noticeable, confirming olein's chemical role. The C=O band of rosin (around 1690 cm^{-1}) broadens and shifts slightly to approximately 1686 cm^{-1}, which suggests possible interactions between ester and carboxyl groups. Additionally, the C–O stretching (around 1170 cm^{-1}) becomes stronger, indicating a rise in ester content. This suggests increased miscibility, where olein's ester groups engage with rosin's acidic parts, producing a more amorphous and flexible matrix [45].

In modified Bioresin C_3, the FTIR spectrum shows the dominance of olein. The ester C=O band at 1743 cm^{-1} becomes prominent. The O–H band is greatly reduced, almost disappearing, which confirms a major drop in hydrogen bonding. The C–H stretching bands (2924/2853 cm^{-1}) show increased strength, indicating the presence of hydrocarbon–rich areas. The rosin C=O band (1685 cm^{-1}) appears broad, suggesting heterogeneous environments due to micro–phase separation. This indicates that higher olein loading leads to over–plasticization, enhancing flexibility while reducing intermolecular cohesion [46].

This specific composition results in a material that is softer and more elastic, making it particularly suitable for cosmetic applications where flexibility and spreadability are essential. However, its reduced crystallinity in comparison to modified Bioresin B suggests a decrease in structural rigidity, rendering it less appropriate for load–bearing uses. This finding is supported by [47], who observed that adding liquid triglycerides to resin matrices improves ductility and softness, although it compromises hardness and heat resistance. Olein functions as a plasticizing agent, diminishing crystallinity and enhancing flexibility within the resin matrix. This composition results in a softer and more elastic material, ideal for cosmetic applications where flexibility and spreadability are desirable [48].

The relationship between FTIR and material strength is indirect yet highly important. FTIR serves as a tool for analyzing chemical properties, which can subsequently be linked to physical and mechanical characteristics, including the material's strength. FTIR aids in comprehending the chemical transformations that contribute to variations in strength. For instance, material modification. When a material undergoes modification, FTIR can verify the establishment of

new bonds or structural alterations that enhance strength. In this research, the modification of resin, palm wax, and olein will yield modified resin A, which consists of resin and palm wax, modified resin B, which includes resin, palm wax, and microwax, and modified resin C, which is composed of resin and olein. Each modified resin generates a distinct type of chemical bond group and strength [49], [50].

FTIR analysis (Figures 1–3) supports the presence and relative strength of physical interactions between rosin and each modifier. The C=O stretching band of rosin (1700–1720 cm^{-1}) shifts slightly to lower wavenumber and broadens in palm–wax–modified samples, consistent with moderate hydrogen–bond formation and increased dipolar coupling. In the B–series, the C=O band frequently appears as a multi–component feature and the CH_2 stretching/rocking modes (2920, 2850, 720 cm^{-1}) sharpen markedly together, indicating increased alkyl–chain ordering and heterogeneous but strong physical interactions (high van der Waals cohesion and constrained hydrogen bonding). In contrast, the C–series spectra show broader O–H/C=O features and attenuated crystalline CH_2 signatures, suggesting olein acts primarily as a plasticizer: it forms weaker dipolar interactions with rosin while disrupting crystalline packing. These FTIR findings corroborate DSC/TGA and mechanical data, supporting the conclusion that microwax introduces the strongest physical reinforcement (B–series), palm wax provides moderate hydrophobic reinforcement (A–series), and olein yields flexible, plasticized matrices (C–series).

Based on the FTIR analysis presented above, modified bioresin B exhibits the most pronounced chemical interactions, leading to enhanced rigidity and thermal stability. Modified bioresin C provides superior flexibility but at the cost of some structural integrity, while modified bioresin A occupies a position between the two. These results highlight the importance of specific combinations of modifiers in customizing resin properties for targeted applications.

3.2 *Thermal analysis*

DSC and TGA analyses were performed to evaluate the thermal behavior and stability of the modified bioresins. The results provide insight into glass transition temperature, melting temperature, and decomposition profile, which are critical for predicting the performance of modified bioresins in biocomposite applications.

3.2.1 DSC–TGA of Modified Bioresin A

Figure 4 shows the DSC–TGA thermograms for modified bioresin A_1, A_2, and A_3. While, Table 1 presents a summary of the values of T_melting (Tm), T_glass transition (Tg) and T_degradation (Td) for modified bioresin A. Table 2 describes relations between relative material change (%) with Tm, Tg, and Td in modified bioresin A.

Table 1: Relationship between heat flow with melting point, transition point and degradation point in modified bioresin A.

Modified Bioresin	T_melting		T_glass transition		T_degradation	
	Temp (°C)	Heat flow (mW)	Temp (°C)	Heat flow (mW)	Temp (°C)	Heat flow (mW)
Bioresin A_1	40	-1.45763	90	-0.954240	370	-29.5752
Bioresin A_2	45	-4.00822	140	-2.94175	395	12.0578
Bioresin A_3	55	-14.00602	230	25.8184	410	38.7079

Table 2: Relations between relative material change with melting point, transition point and degradation point in modified bioresin A.

Modified Bioresin	T melting		T glass transition		T degradation	
	Temp (°C)	Material Change (%)	Temp (°C)	Material Change (%)	Temp (°C)	Material Change (%)
Bioresin A_1	40	-0.000165	90	-0.8156	370	-99.2722
Bioresin A_2	45	-0.271316	140	-0.51127	395	-89.179
Bioresin A_3	55	-0.316543	230	-1.147026	410	-93.8764

The DSC thermogram of modified bioresin A_1 revealed a distinct endothermic melting peak at 40 °C, attributed to the melting of palm wax crystalline domains dispersed within the amorphous rosin matrix. The relatively sharp nature of this peak compared to pure rosin, which does not display any low-temperature crystalline transitions, confirms that palm wax effectively introduces crystalline order into the system [51]. This crystalline reinforcement reduces brittleness and provides localized rigidity, while the

relatively low intensity of the peak (compared to modified bioresin A_2 or A_3) reflects the limited crystalline fraction at only 5% palm wax addition.

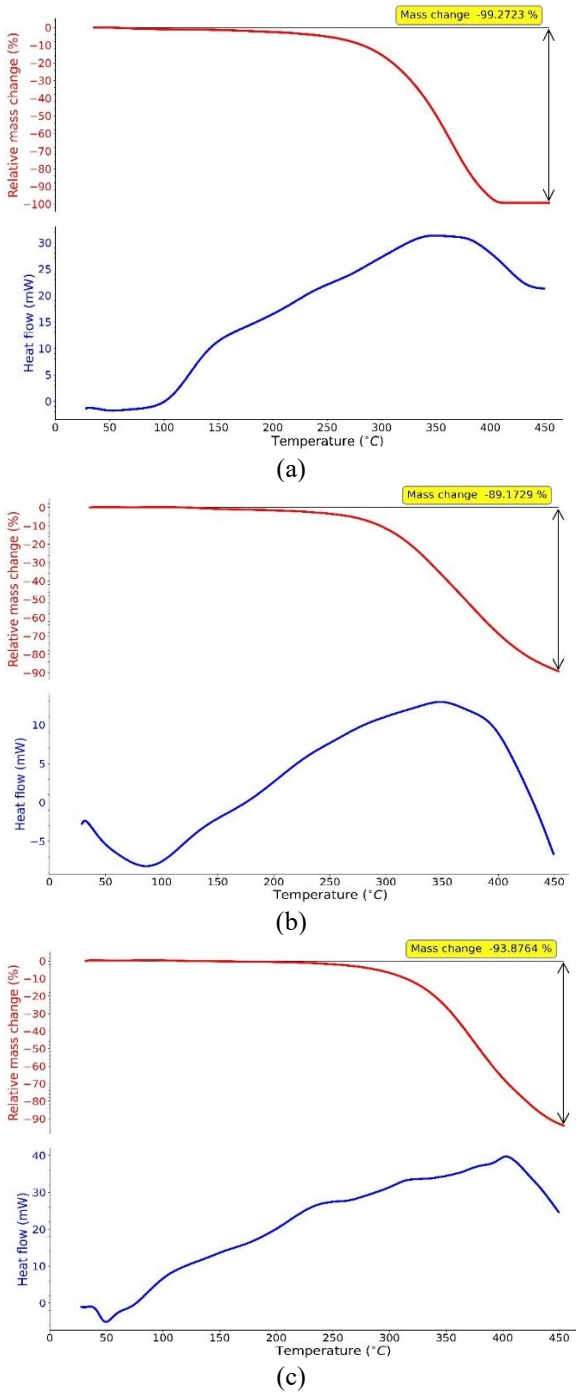

Figure 4: DSC–TGA analysis of (A: Bioresin A1), (B: Bioresin A2), and (C: Bioresin A3).

The TGA profile showed that modified bioresin A_1 exhibited an onset degradation temperature of around 370 °C, which is higher than pure rosin (215–295 °C), indicating an improvement in thermal resistance. The relative material change was–99.2722%, suggesting that palm wax incorporation contributed to more stable decomposition intermediates and reduced volatilization.

Overall, the addition of 5% palm wax in modified bioresin A_1 moderately enhanced the thermal stability of rosin, primarily through the formation of crystalline regions that stabilized the polymeric backbone during thermal stress. However, the improvement was less pronounced than modified bioresin A_2, which exhibited higher Tg, Td, and residue.

The DSC curve of modified bioresin A_2 showed a well–defined glass transition at around 140 °C, which corresponds to the melting of palm wax crystalline domains. Compared to modified bioresin A_1, the increase in palm wax content to 10% produced a sharper and slightly higher melting peak, confirming the reinforcement of crystalline order within the rosin matrix. This observation suggests that a higher palm wax concentration leads to a more significant crystalline contribution, which is consistent with wax–rich composites where increased crystallinity improves rigidity and barrier performance [52].

The relative material change was around –89.179%, which is greater than modified bioresin A_1. This improved char formation suggests that palm wax not only increases crystalline stability but also contributes to the generation of thermally stable residues, an advantage for applications requiring high thermal resistance and oxidative durability.

When compared to pure rosin, which typically shows thermal degradation at 215–295 °C [53], modified bioresin A_2 demonstrates significant improvements in both thermal stability and structural integrity. The higher crystallinity imparted by 10% palm wax further reduces the brittleness of pure rosin, while providing better resistance to thermal decomposition.

Overall, modified bioresin A_2 shows superior thermal performance and structural reinforcement compared to modified bioresin A_1. These characteristics make A_2 particularly promising for applications where rigidity, barrier strength, and high–temperature stability are crucial, such as fruit coatings requiring oxidative resistance, or packaging films designed for extended shelf life.

The DSC thermogram of modified bioresin A_3 displayed an endothermic transition around 55 °C, which corresponds to the melting of palm wax crystalline regions. Compared with modified bioresin A_1 and A_2, the melting peak in A_3 became more pronounced and shifted slightly to a higher temperature, confirming that increasing palm wax loading enhances crystalline ordering within the rosin matrix. This reinforces the role of palm wax as a crystallinity–promoting additive, which improves rigidity and dimensional stability [11].

The TGA curve revealed a major mass loss of around 93.8764%, occurring primarily at 410 °C. Tg was approximately 230 °C, which is higher than A_1 (90 °C) and A_2 (140 °C), suggesting that the addition of 15% palm wax further delays the initial decomposition of the resin. Td was observed on 410 °C, higher than A_1 (370 °C) and A_2 (395 °C). This indicates that increasing palm wax concentration improves the thermal stability of the resin by reinforcing the matrix with crystalline domains that act as thermal barriers.

Interestingly, the residual mass decreased to approximately -93.8764%, which is lower than A_2. This reduction suggests that at high palm wax loading, the increased hydrocarbon–rich content of palm wax results in more volatile decomposition products and reduced char yield, despite enhancing crystalline stability during heating. Thus, while palm wax improves Tg and Td, excessive addition reduces char stability, reflecting a trade–off between crystallinity reinforcement and final residue formation.

In summary, modified bioresin A_3 exhibited the highest Tg and Td among the modified bioresin A–series, confirming superior thermal resistance. However, its reduced char residue compared with A_2 highlights that there may be an optimal palm wax loading beyond which additional content does not proportionally enhance overall thermal robustness. These findings are particularly relevant for applications requiring thermal durability but not necessarily high char yield, such as biodegradable packaging films and coatings.

For the modified bioresin A–series, Td values ranged from 370–410 °C, showing slight variation with palm wax loading. The incorporation of 5% palm wax (Bioresin A_1) reduced Td (370 °C, -29.6 mW), consistent with a plasticization effect that increases chain mobility [54]. Interestingly, bioresin A_2 (10% palm wax) and bioresin A_3 (15% palm wax) both displayed higher Tg (140 °C, -2.94175 mW and 230 °C, 25.8184 mW, respectively), suggesting enhanced intermolecular interactions and denser packing at higher palm wax ratios. The melting transitions gradually increased from 40 °C (A_1) to 55 °C (A_3), indicating improved crystalline ordering with increasing palm wax content.

Thermal degradation shifted toward higher values at 410 °C for A_3, compared to 370 °C in A_1, reflecting improved thermal stability with higher wax incorporation. Td for modified bioresin A was 370–410 °C, higher than that of pure rosin (215–295 °C), confirming enhanced thermal stability due to palm wax incorporation. This improvement is beneficial for packaging and food–contact composites where thermal processing is required [55]. DSC analysis revealed a glass transition at 90–230 °C and a Tm of 40–55 °C, reflecting the crystalline contribution of palm wax. These transitions enhance rigidity and thermal endurance, supporting applications in packaging where moderate heat resistance is required [56].

3.2.2 DSC–TGA of Modified Bioresin B

Figure 5 shows the DSC–TGA thermograms for modified bioresin B_1, B_2, and B_3. Table 3 presents a summary of the values of Tm, Tg, and Td for modified bioresin B and Table 4 describes relations between relative material change with Tm, Tg and Td in modified bioresin B.

Table 3: Relationship between heat flow with melting point, transition point and degradation point in modified bioresin B.

Modified Bioresin	T_melting		T_glass transition		T_degradation	
	Temp (°C)	Heat flow (mW)	Temp (°C)	Heat flow (mW)	Temp (°C)	Heat flow (mW)
Bioresin B_1	90	-4.16873	150	-17.013	400	36.8167
Bioresin B_2	40	-3.73254	60	-7.89598	390	23.1436
Bioresin B_3	60	-7.06726	180	-0.208859	370	7.50604

Table 4: Relations between relative material change with melting point, transition point and degradation point in modified bioresin B.

Modified Bioresin	T melting		T glass transition		T degradation	
	Temp (°C)	Material change (%)	Temp (°C)	Material change (%)	Temp (°C)	Material change (%)
Bioresin B_1	90	-1.36349	150	-0.454073	400	-91.4886
Bioresin B_2	40	-0.011479	60	-0.49633	390	-86.5021
Bioresin B_3	60	-0.004054	180	-0.6411	370	-99.9642

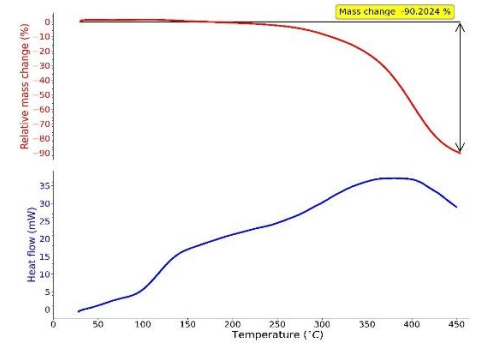

(A)

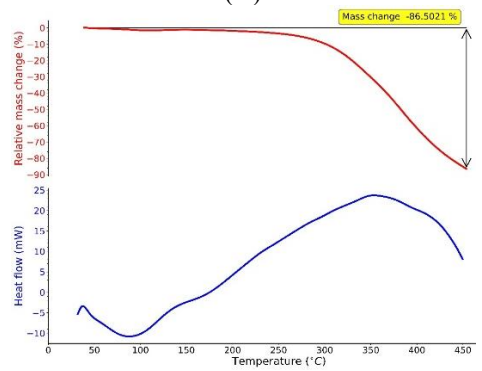

(B)

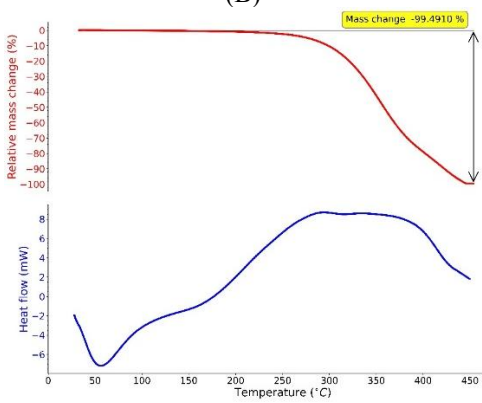

(C)

Figure 5: DSC–TGA analysis of (A: Bioresin B1), (B: Bioresin B2), and (C: Bioresin B3).

The incorporation of palm wax and microwax in different proportions (5, 10, and 15%) significantly modified the thermal response of modified bioresin, as revealed in the DSC–TGA thermograms (Figure 5). The DSC thermogram of modified bioresin B_1 displayed two overlapping endothermic peaks in the low–temperature region: one at 63–68 °C attributed to palm wax melting, and another at 72–76 °C associated with microwax crystallites.

The dual–peak behavior suggests multimodal crystalline populations, which provide heterogeneous nucleation sites within the resin. The TGA curve revealed Tg 150 °C, with Td at 400 °C. The residual material change was around -91.4886%, indicating enhanced carbonization due to wax incorporation.

Increasing the wax content to 10% (Modified bioresin B_2) broadened the melting endotherm into a less distinct region between 60–75 °C, reflecting overlapping crystallite melting. This blending effect suggests partial miscibility between palm wax and microwax, which reduces the sharpness of individual melting signals. T–glass transition was 60 °C, with T–degradation shifting to around 390 °C, showing a stabilization effect. Residual mass increased to approximately -86.5021%, likely due to more volatile wax decomposition competing with char formation.

In bioresin B_3, the DSC showed a broader but weaker endothermic transition spanning 60–78 °C, with the microwax contribution largely suppressed. This indicates disruption of crystalline order at higher loadings, producing more amorphous domains. TGA data revealed Tg of 180 °C and Td at around 370 °C.

The modified bioresin B-series exhibited Tg values between 60–180 °C, with the highest Tg observed in modified bioresin B_3 (180 °C, -0.208859 mW). The addition of microwax influenced both crystallinity and chain rigidity. A modest addition of 5% microwax (Bioresin B_1) yielded Tg at 150 °C, and higher incorporation (15%) increased Tg, confirming a reinforcement effect from the long–chain hydrocarbons of microwax [57]. Melting temperatures ranged from 40–90 °C, with heat flow values suggesting partial crystallinity.

Overall, the results demonstrate that balanced incorporation of palm wax and microwax enhances both crystallinity and thermal stability, with 10% wax

loading (Bioresin B_2) emerging as the most favorable compromise between stability and structural integrity. The presence of two transitions confirms that palm wax and microwax crystallites coexist in the matrix, yielding multimodal crystallite populations. This broadened melting profile is advantageous for tuning softening characteristics in biocomposite applications. The TGA results were consistent with a one–step thermal degradation pathway, with total mass losses exceeding 90% and Td around 390 °C.

3.2.3 DSC–TGA of Modified Bioresin C

Figure 6 shows the DSC–TGA thermograms for modified bioresin C_1, C_2, and C_3. Table 5 presents a summary of the values of Tm, Tg, and Td for modified bioresin C and Table 6 describes relations between relative material change with Tm, Tg and Td in modified bioresin C.

Table 5: Relationship between heat flow with melting point, transition point and degradation point in modified bioresin C.

Modified Bioresin	T_melting		T_glass transition		T_degradation	
	Temp (°C)	Heat flow (mW)	Temp (°C)	Heat flow (mW)	Temp (°C)	Heat flow (mW)
Bioresin C_1	50	-5.57669	190	-9.80042	400	33.8086
Bioresin C_2	50	-0.17777	190	-0.89145	390	64.2556
Bioresin C_3	50	-0.3996	180	-23.2485	390	41.2769

Table 6: Relations between relative material change with melting point, transition point and degradation point in modified bioresin C.

Modified Bioresin	T melting		T glass transition		T degradation	
	Temp (°C)	Material change (%)	Temp (°C)	Material change (%)	Temp (°C)	Material change (%)
Bioresin C_1	50	-0.011688	190	-1.34039	450	-98.0321
Bioresin C_2	50	-2.54792	190	-13.0748	450	-81.2156
Bioresin C_3	50	-0.593391	180	-0.88466	450	-99.9642

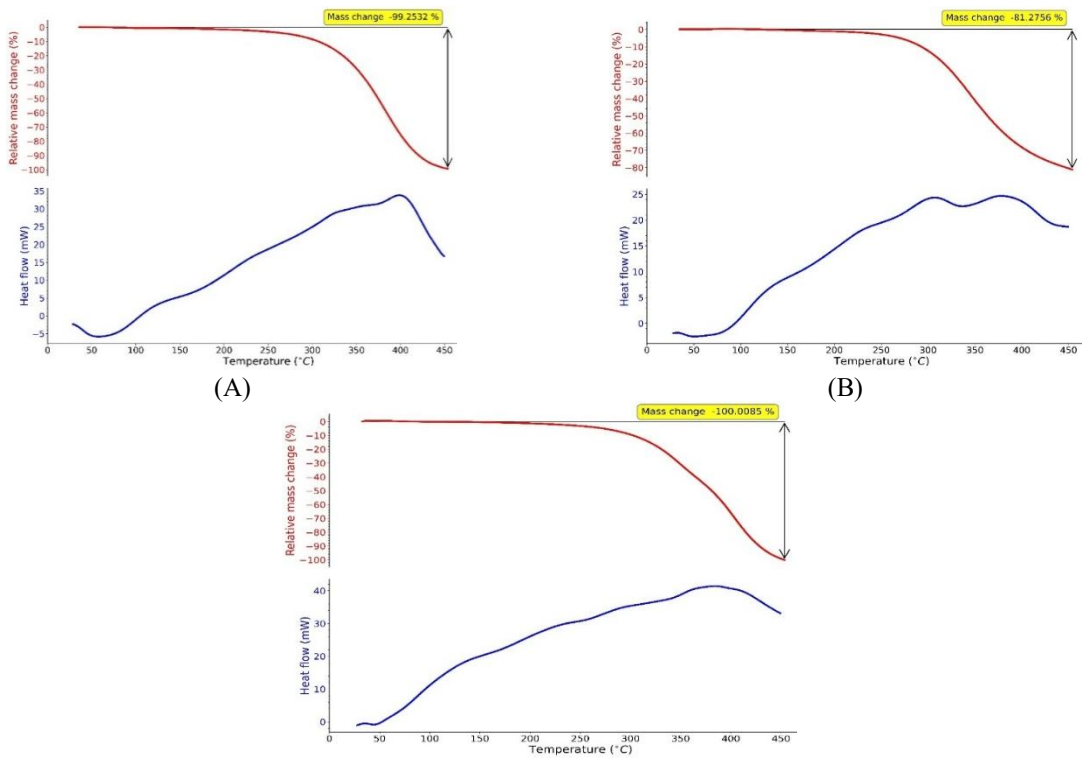

Figure 6: DSC–TGA analysis of (A: Bioresin C_1), (B: Bioresin C_2), and (C: Bioresin C_3).

Modified bioresin C exhibited a markedly different behavior. The incorporation of olein into rosin produced distinct modifications to the thermal and structural properties of the resulting bioresins. Unlike crystalline wax modifiers, olein is a liquid triglyceride that acts primarily as a plasticizer, reducing molecular packing and weakening crystalline order.

DSC thermograms revealed that all modified bioresin C–series formulations exhibited weak or absent melting endotherms compared to the sharper transitions of palmwax– or microwax–modified systems. In modified bioresin C_1, a broad thermal event was still observable, but at bioresin C_2 and especially bioresin C_3, the signal became diffuse, indicating a progressive transition toward an amorphous structure. This suppression of crystallinity is consistent with olein's liquid nature, which disrupts regular molecular packing and enhances chain mobility within the resin matrix.

Thermogravimetric analysis showed that olein incorporation reduced thermal stability relative to pure rosin and other bioresin series. Tm for modified bioresin C_1, C_2 and C_3 was 50 °C. Tg was 190 °C (Bioresin C_1), 190 °C (Bioresin C_2) and 180 °C (Bioresin C_3). This downward trend confirms that olein lowers the resistance of the resin matrix to thermal decomposition.

Relative material change for modified bioresin C_1, C_2, and C_3 was -98.0321%, -81.2156% and -99.9642%, respectively, reflecting the volatile and oxidative susceptibility of olein. Unlike palmwax or microwax, olein contributed little to char formation, indicating that its thermal degradation pathway favors volatilization over stable residue generation.

The results highlight a clear plasticizing effect of olein on rosin bioresins. While thermal resistance is compromised, the enhanced amorphous character may provide benefits in terms of flexibility, toughness, and processability. Such properties could be advantageous for applications requiring softer, more ductile matrices rather than rigid, heat–resistant systems. In this context, olein–modified bioresins are not optimized for high–temperature applications but may serve well as flexible binders or coatings in biocomposites, complementing the stiffer, more crystalline matrices of palmwax and microwax-based systems.

Unlike the wax-containing systems, no sharp low–temperature melting peak was detected. Instead, the DSC curve showed a smooth, broad baseline shift in the 40–80 °C range, consistent with plasticizer–induced softening rather than crystalline melting. Olein, being a liquid triglyceride, disrupts crystalline packing and enhances the amorphous fraction, leading to increased chain mobility of the rosin matrix. This confirms olein's role as a plasticizer rather than a crystallinity inducer. The TGA thermogram indicated Tg 180–190 °C and Td around 450 °C.

Overall, the DSC–TGA results demonstrate that the type of modifier strongly influences the low–temperature thermal response of the bioresins. Palm wax and microwax contribute sharp melting peaks, indicative of crystalline microdomains, whereas olein suppresses crystallinity and induces amorphous plasticization. In all cases, the resins retained good thermal stability with Tg values above 190 °C, supporting their potential utility as biobased matrices for thermally processed biocomposites.

The melting, glass transition, and degradation behavior of the modified bioresins show clear structural differences driven by the type of modifier added to rosin. In the modified bioresin A, melting temperatures were low to moderate (40–55 °C across A_1–A_3), with corresponding heat flow values of -1.46 to -4.01 mW. These modest endotherms reflect the formation of semi–crystalline domains contributed by palm wax. The glass transition temperatures increased substantially with formulation concentration (A_1: 90 °C, A_2: 140 °C, A_3: 230 °C), indicating enhanced molecular packing as palm–wax crystallinity developed. The degradation temperatures (370–410 °C) further confirm increased thermal resistance in higher–palm–wax variations. This behavior aligns with palm wax's long–chain esters forming ordered domains that stabilize the matrix.

In the modified bioresin B, the highest melting temperatures among all samples were observed in B_1 (90 °C) and B_3 (60 °C), with ΔH values reaching -7.07 mW in B_3, indicating a dense crystalline structure. Microcrystalline wax strengthens crystallization networks, and this is reflected in the moderately high glass transition temperatures (B_1: 150 °C, B_3: 180 °C) and high degradation temperatures (B_1: 400 °C, B_3: 390 °C). These formulations also show stronger thermal stability than the A–series, particularly B_1 and B_3, which reached 400 °C and 390 °C before degradation. Even B_2, which combines low melting temperature (40 °C) and low Tg (60 °C), still maintained a relatively stable Td (370 °C). Collectively, the B–series numerical data confirm that microcrystalline wax substantially reinforces the internal structure.

The modified bioresin C exhibited lower melting temperatures (50 °C for all samples) and significantly

lower heat flow values in some samples (C_2: -0.18 mW, C_3: -0.40 mW), consistent with reduced crystallinity. Olein, functioning as a plasticizer, disrupted crystal formation and decreased structural rigidity. Although Tg values remained relatively high (180–190 °C), the endothermic transitions were broad and shallow, indicating amorphous or loosely packed structures. Degradation temperatures ranged from 390–400 °C, showing that olein does not compromise high–temperature decomposition resistance but does soften the matrix substantially. These numerical trends establish a consistent pattern: B–series > A–series > C–series in crystalline reinforcement, with melting temperatures ranging from 40 to 90 °C, Tg from 60 to 230 °C, and Td from 370 to 410 °C depending on modifier chemistry.

4 Structure–Property Relationships

The relationships between the resin structure (rosin backbone), modifiers (palm wax, microwax, olein), and the resulting properties can be summarized as follows:

In modified bioresin A–series, palm wax increases crystallinity and intermolecular packing. This shifts Tg from 90 °C to 230 °C and Tm from 40 °C to 55 °C. Higher crystallinity corresponds to improved hardness (A_3 harder than A_1). This demonstrates that palm wax primarily controls rigidity and crystallinity.

In modified bioresin B–series, microwax can either: integrate into crystalline regions to increase mechanical rigidity (B_1: 8.22 ± 5.25 kg hardness, Tg:150 °C, Tm: 90 °C), and disrupt packing to softer structures (B_2: 13.12 ± 10.43 kg hardness, Tg: 60 °C). Thus, microwax behaves as a dual–function modifier, making B–series highly tunable for different performance targets.

In modified bioresin C–series, olein could reduce crystallinity, maintain high Tg (180–190 °C) due to rigid rosin backbone, and produce wide mechanical variability (hard C_1 to very soft C_3). This indicates olein acts as a plasticizing network modifier that selectively reduces structural coherence.

The thermal and structural analysis of the modified bioresins (Formulations A, B, and C) revealed a distinct correlation between their physicochemical properties and potential application performance. The DSC results showed that formulation A exhibited the lowest melting point temperature (40–55 °C) and moderate glass transition (90–230 °C) with relatively high heat flow of melting (-1.5 to - 4 mW), indicating a semi–crystalline yet flexible matrix. This balance provides good film–forming ability and desirable flexibility, making formulation A suitable for cosmetic applications such as lip balms or ointments, where softening near body temperature is advantageous. In contrast, formulation B presented slightly higher Tg (60–180 °C) and Tm (40–90 °C), together with improved thermal stability (Td onset ≈ 370–400 °C), suggesting stronger molecular cohesion and enhanced rigidity. These properties are beneficial for coating materials that require structural integrity, gloss, and heat resistance under moderate exposure. Meanwhile, formulation C exhibited the highest Tg (≈ 180–190 °C) and Tm (50 °C) with a lower ΔH, implying a denser and more amorphous network with limited molecular mobility. The high degradation temperature (Td 450 °C) confirms superior thermal stability, which is desirable for biodegradable packaging films that must endure heat–sealing and storage conditions. Overall, the progressive increase in Tg, Tm, and Td values from formulation A to C reflects increasing rigidity and crosslink density, which directly enhance performance requirements across target applications, soft and flexible, for cosmetics, intermediate rigidity for coatings, and thermally stable for packaging materials. This demonstrates a clear property–performance correlation that supports the rational design of bioresin formulations for specific functional uses.

The thermal and mechanical behavior of bioresin B exhibited positive deviation from the linear rule of mixtures when compared to bioresin A (rosin + palm wax) and the theoretical additive performance of its components. Based on DSC and TGA analyses, the incorporation of microwax into the rosin–palm wax matrix increased Tg from 90 °C in bioresin A_1 to 150 °C in bioresin B_1, and Tm from 40 °C to 90 °C, while the degradation onset temperature (Tonset) also rose from 370 °C to 400 °C. Such an improvement exceeds the prediction of a simple compositional average, indicating enhanced cohesive interactions among crystalline and amorphous domains. This synergistic stabilization is likely attributed to the compatibility between the long–chain hydrocarbons of microwax and the resin acids of rosin, which enhances van der Waals packing and restricts chain mobility. In terms of mechanical response, the penetration value decreased from 15.06±12.82 kg penetration (A_2) to 8.22 ± 5.25 kg (B_2), reflecting a stiffer and less deformable surface. Taken together, the combination

of higher Tg, Tm, and hardness with moderate thermal stability improvement suggests that bioresin B achieves an optimal balance between rigidity and thermal endurance, suitable for coating or packaging applications requiring both strength and heat resistance.

5 Hardness

The hardness value of the modified bioresin is presented in Figure 7. The hardness testing outcomes for Modified Bioresin A_1 were recorded as 13.26±12.17 kg, while for A_2, it increased to 15.06±12.82 kg, and for A_3, it decreased to 11.63±4.30 kg. This information implies that a higher quantity of palm wax results in a reduction of the hardness value.

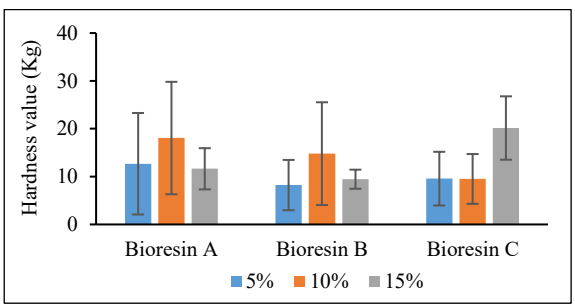

Figure 7: hardness value of modified bioresin A-C.

In the context of modified bioresin B, the hardness measurement for modified bioresin B_1 was noted at 8.22±5.25 kg, B_2 was noted at 13.12 ±10.43 kg, and B_3 was noted at 9.45±1.99 kg. This data suggests that increasing the amount of palm wax in conjunction with microwax leads to a diminished hardness value.

Regarding modified bioresin C, the hardness measurement for modified bioresin C_1 was 9.47±5.61 kg, for C_2 it remained at 9.47±4.65 kg, and for C_3 it was 9.47±8.10 kg. This information demonstrates that a rise in the quantity of palm olein is associated with an increase in the hardness value.

5.1 *Hardness of modified bioresin A*

The hardness values of modified bioresins A did not increase linearly with palm wax concentration. At 5% palm wax addition, the hardness increased slightly compared to pure rosin, while 10% palm wax yielded the highest hardness values. Interestingly, when the concentration was increased to 15%, the hardness decreased below that of the 5% and 10% formulations.

At low levels of palm wax (5–10%), wax crystals can disperse within the rosin matrix and act as reinforcing domains, improving rigidity. This contributes to higher hardness because the wax reduces molecular mobility and enhances intermolecular interactions between resin acids and the long-chain aliphatic structures of wax. Comparable reinforcement effects of crystalline wax particles within polymer matrices have been reported, indicating that moderate wax loading increased rigidity in composite systems by restricting chain mobility [58].

Beyond a threshold, excess palm wax may no longer be well–dispersed but instead form aggregated crystalline domains. These domains can act as “soft inclusions” within the rigid rosin network, lowering hardness. In addition, the long-chain hydrocarbons in palm wax can function as plasticizers at higher concentrations, increasing free volume and molecular mobility. This behavior is consistent with a previous study that indicated the excessive wax addition in resin–wax formulations promotes plasticization and reduces hardness [59]. An optimum concentration of palm wax (10%) enhances hardness by reinforcing the rosin matrix and reducing chain mobility, but higher concentrations (15%) reverse this effect due to plasticization and phase separation.

5.2 *Hardness of modified bioresin B*

The hardness behavior of the B–series modified bioresins demonstrates a non–linear relationship with increasing palm wax and microwax content. Modified bioresin B_1 exhibited moderate hardness due to the initial reinforcement of the rosin matrix by crystalline wax domains. Modified bioresin B_2 showed the highest hardness values, indicating an optimal concentration where crystalline phases from both palm wax and microwax interact synergistically with rosin. This promotes tighter molecular packing and increases microstructural stiffness. Modified bioresin B_3, however, displayed reduced hardness compared to B_2 and even lower than B_1 in some replicates. This decline is likely due to phase separation and excessive crystallite aggregation, which weakens the interfacial adhesion between the crystalline domains and the amorphous rosin matrix. As a result, stress is not efficiently transferred across the phases, leading to embrittlement and reduced surface hardness.

The modified bioresin B_2 provides an optimal balance between crystalline reinforcement and matrix compatibility, explaining its superior hardness. Too

little wax in modified bioresin B_1 gives insufficient reinforcement, while too much wax in modified bioresin B_3 introduces phase separation and embrittlement, lowering hardness.

5.3 *Hardness of modified bioresin C*

The hardness value observed in the C–series shows a nonlinear relationship with increasing olein concentration. Modified bioresin C_1, recorded hardness value 9.57, C_2: 9.47, and C_3: 17.89.

Olein is a triglyceride that functions as a natural plasticizer, increasing molecular free volume and chain mobility. In modified bioresin C_1 and C_2, olein reduces intermolecular hydrogen bonding between rosin acids, which lowers rigidity and hardness compared to pure rosin. This explains why hardness decreases from C_1 to C_2. Similar effects have been reported in bioresin and polymer systems where oils or fatty acid esters act as plasticizers, reducing hardness and increasing flexibility [60].

In modified bioresin C_3, instead of further softening, the system shows a relative increase in hardness. This paradox may arise from Oleic crystallite formation, which can act as a reinforcing filler. Reduced miscibility at higher olein, leading to phase separation that contributes to hardness in localized regions. Comparable phenomena have been observed in natural resin/oil composites, where higher fatty acid or oil content leads to crystallization, improving stiffness despite overall plasticization [61].

The hardness profile reflects the balance between plasticization at low olein concentration (5–10%) and microcrystalline reinforcement at higher concentration (15%). This explains why hardness initially drops but then partially recovers in the C_3 sample, albeit with higher variability.

The graph presented in Figure 7 depicts two key aspects: 1) the average value represented by the height of the bars, and 2) the consistency of the data indicated by the length of the error bars. The analysis of the average bar height reveals that the most challenging sample is modified bioresin C at 15%, which exhibits the highest average hardness value of approximately 20.15. Furthermore, a distinct trend is observed in modified bioresin C: as the concentration increases, the hardness of the bioresin also increases (hardness at 15% > 10% > 5%). In contrast, the hardness trends for modified bioresin A and B are inconsistent. The T line (error bars) for modified bioresin B at 15% is notably short, indicating that the five replicate data points are closely aligned, suggesting consistency and reliability in this data. Conversely, the longer lines for modified bioresin A and modified bioresin C signify a greater variability in their values. From this analysis, it can be concluded that there is no statistically significant difference in the hardness values among the samples of modified bioresin A, B, and C. This indicates that the various types of additives (Palm wax, Microwax, Olein) do not have a demonstrable impact on hardness. Additionally, the different concentrations (5%, 10%, 15%) also do not appear to influence hardness. There is no observed interaction effect between the type of additive and its concentration.

The modified bioresin, as revealed in this research, reveals distinct structure–property relationships that highlight the innovative aspects of this study. In contrast to earlier investigations that concentrate on single–component natural waxes or straightforward blends, this research methodically illustrates how combinatorial formulation strategies, incorporating rosin, palm wax, microcrystalline wax, and olein, can be employed to deliberately adjust thermal transitions, degradation characteristics, and hardness performance.

A significant innovative element is the discovery that each structural modifier yields a unique functional signature, facilitating predictive tuning of material properties. For instance, the addition of microcrystalline wax in the B–series markedly raises the melting point (up to 90 °C) and glass transition temperature (150–180 °C), affirming its function as a crystalline reinforcement phase. This synergistic effect, where performance surpasses the expectations set by the rule–of–mixtures, illustrates that microcrystalline wax enhances both rigidity and thermal stability beyond the capabilities of palm wax or rosin alone. This finding offers a novel perspective that has not been explicitly quantified in prior literature.

The C–series proves another innovative contribution: olein–induced structural densification, where higher levels of olein improve mechanical hardness (up to 17.89±8.10 kg in C_3). This challenges the traditional belief that liquid oils invariably function as plasticizers. Conversely, the research findings reveal a distinctive phenomenon where olein enhances chain packing at elevated loadings, leading to increased formulation stiffness despite its liquid form. Such behavior signifies a substantial advancement in comprehending the dynamics of mixed resin–oil systems.

The A–series, characterized by palm wax and rosin, illustrates that semi–crystalline matrices can be designed to optimize thermal and mechanical performance, with Tg values ranging from 90 °C to 230 °C and hardness levels between 12–18 kg. The capacity to achieve such varied performance metrics represents a significant achievement in the field.

The relationship between melting behavior, ΔH, Tg, Td, and hardness becomes clear when numerical values are compared. Highest crystallinity is seen in the B–series, with melting up to 90 °C, ΔH up to -7.07 mW, Tg up to 180 °C, Td up to 400 °C, and hardness value (8.22±5.25 to 13.12±10.43 kg). The B series indicates the most rigid and thermally resistant.

Moderate crystallinity is seen in the A-series, with Tm 40–55 °C, ΔH -1.46 to -4.01 mW, Tg 90–230 °C, Td 370–410 °C, penetration (11.63±4.30 to 15.06±12.82 kg). The A series show a balanced rigidity and flexibility. Reduced crystallinity is seen in the C–series, with Tm 50 °C, ΔH as low as -0.18 mW, Td 390–400 °C, and hardness value (9.47±4.65 to 17.89±8.10kg). The C series become softest and most ductile.

The direct numerical correlation confirms: higher melting temperature and ΔH will become higher hardness. Meanwhile, lower ΔH and constant low melting will produce softer material. Accordingly: B–series is best suited for rigid coatings, structural waxes, or protective films. A–series fits applications requiring moderate stiffness (e.g., printing inks, intermediate coatings). C–series aligns with flexible packaging, cosmetics, and formulations requiring softness and spreadability.

6 Conclusions

This study introduces a renewable, customizable bioresin system based on rosin modified with palm wax, microwax, and olein, aimed at replacing petroleum-derived waxes and resins in sustainable packaging, coating, and cosmetic applications. The innovative aspect lies in tunable thermal–mechanical performance derived solely from biobased modifiers, enabling precise control of melting point (40–90 °C), glass transition (60–230 °C), hardness (8.22 ± 5.25 kg to 17.89 ± 8.10 kg), and thermal degradation stability (370–410 °C). Unlike previous studies that report single-component bioresins, this work demonstrates a structure–property design strategy where crystallinity, molecular mobility, and cohesive energy density can be engineered through modifier selection.

Palm wax enhanced crystalline rigidity (Modified Bioresin A-series), microwax provided dual-function structuring or plasticizing behavior (Modified Bioresin B-series), and olein enabled flexible phase-modified networks (Modified Bioresin C-series), showing that formulations can be tailored for specific end-use functions. The resulting materials are thermally robust (Td ≥ 370 °C), mechanically competitive with synthetic resins, and based entirely on renewable feedstocks. These findings position the modified bioresins as viable candidates for biodegradable packaging films, cosmetic matrices, and surface-protection coatings, while highlighting scalable pathways for green materials engineering.

Acknowledgments

The authors would like to acknowledge National Research and Innovation Agency (BRIN) for supporting this research through internal research program funds.

Author Contributions

S.A.: conceptualization, methodology; investigation; writing; A.Y.: investigation, methodology; W.H.: research design; F.: investigation, data analysis; A.S.: investigation; L.J.: writing-reviewing and editing; F.A.S.: writing-reviewing; E.S.H.: investigation; K.: investigation; B.: investigation; A.K.: investigation. All authors have read and agreed to the published version of the manuscript.

Conflicts of Interest

The authors declare no conflict of interest.

Declaration of generative AI and AI-assisted technologies in the writing process

The authors utilized the ChatGPT tool to enhance the language and readability of the manuscript.

References

[1] Y. F. Lei, X.-L. Wang, B.-W. Liu, X.-M. Ding, L. Chen, and Y.-Z. Wang, "Fully bio-based pressure-sensitive adhesives with high adhesivity derived from epoxidized soybean oil and rosin acid," *ACS Sustainable Chemistry & Engineering*, vol. 8, no. 35, pp. 13261–13270,

Aug. 2020, doi: 10.1021/acssuschemeng.0c03451.

[2] L. Vevere, A. Fridrihsone, M. Kirpluks, and U. Cabulis, "A review of wood biomass-based fatty acids and rosin acids use in polymeric materials," *Polymers*, vol. 12, no. 11, Nov. 2020, Art. no. 2706, doi: 10.3390/polym12112706.

[3] J. Wang, S. Liu, J. Yu, C. Lu, C. Wang, and F. Chu, "Rosin-derived monomers and their progress in polymer application," in *Sustainable Polymers from Biomass*, USA: Wiley, Feb. 2017, pp. 103–149, doi: 10.1002/9783527340200.ch6.

[4] V. Mahendra, "Rosin product review," *Applied Mechanics and Materials*, vol. 890, pp. 77–91, Apr. 2019, doi: 10.4028/www.scientific.net/AMM.890.77.

[5] S. Kugler, P. Ossowicz, K. M. Matusiak, and E. Wierzbicka, "Advances in rosin-based chemicals: The latest recipes, applications and future trends," *Molecules,* vol. 24, no. 9, Apr. 2019, Art. no. 1651, doi: 10.3390/molecules24091651.

[6] M. Mardiah, Y. A. Situmorang, A. Aqsha, T. W. Samadhi, W. Wulandari, and A. Indarto, "Enhancement of glycerol rosin ester conversion using zeolite-based catalyst," *Case Studies in Chemical and Environmental Engineering*, vol. 10, Dec. 2024, Art. no. 101023, doi: 10.1016/j.cscee.2024.101023.

[7] J. Sun, J. Bai, and J. Li, "The synergistic toughening and strengthening effects of cork particles and nanocellulose on rosin-based epoxy resin," *Polymers*, vol. 14, no. 23, Oct. 2022, Art. no. 5064, doi: 10.3390/polym14235064.

[8] F. A. M. M. Gonçalves, M. Santos, T. Cernadas, P. Ferreira, and P. Alves, "Advances in the development of biobased epoxy resins: Insight into more sustainable materials and future applications," *International Materials Reviews*, vol. 67, no. 2, pp. 119–149, Feb. 2022, doi: 10.1080/09506608.2021.1915936.

[9] N. B. Samarth and P. A. Mahanwar, "Modified vegetable oil based additives as a future polymeric material," *Open Journal of Organic Polymer Materials*, vol. 5, no. 1, Jan. 2015, doi: 10.4236/ojopm.2015.51001.

[10] N. Azmi, S. M. Radzi, M. M. Rehan, and N. A. M. Amin, "A review on cosmetic formulations and physicochemical characteristics of emollient and day cream using vegetable based-wax ester," *Malaysian Journal of Science Health & Technology*, vol. 8, no. 2, pp. 38–45, Aug. 2022, doi: 10.33102/mjosht.v8i2.291.

[11] Z. Zhao, C. Qin, X. Piao, Y. Yan, Y. Cao, Z. Wang, and C. Jin, "Improving the hydrophobicity, dimensional stability and mold resistance of bamboo by paraffin/microcrystalline wax/stearic acid modification," *Construction and Building Materials*, vol. 414, Feb. 2024, Art. no. 134902, doi: 10.1016/j.conbuildmat.2024.134902.

[12] M. N. W. Rusli, A. A. B. Leksono, N. J. Jusoh, S. A. Samsudin, J. Jamaluddin, J. C. Lai, and N. Adrus, "Shape memory, naturally enhanced: Epoxidized palm olein in bio-based polylactic acid/polycaprolactone," *Chemistry Select*, vol. 10, no. 25, Jun. 2025, doi: 10.1002/slct.202405078.

[13] U. Dubey and K. Panneerselvam, "Thermally stable, low-combustion and high-strength natural oil-blended epoxy resin," *Polymer International*, vol. 74, no. 5, pp. 444–451, Jan. 2025, doi: 10.1002/pi.6746.

[14] M. Dobrosielska et al., "Effect of wax additives and silanization of diatom surfaces on thermomechanical properties of polylactide composites," *Polymers*, vol. 14, no. 24, Dec. 2022, Art. no. 5511, doi: 10.3390/polym14245511.

[15] T. Saha, M. E. Hoque, and T. Mahbub, "Biopolymers for sustainable packaging in food, cosmetics, and pharmaceuticals," in *Advanced Processing, Properties, and Applications of Starch and Other Bio-based Polymers*, F. M. Al-oqla and S. M. Sapuan, Eds., New York: Elsevier, 2020, pp. 197–214, doi: 10.1016/B978-0-12-819661-8.00013-5.

[16] G. Joshi and K. S. Yadav, "Applications of bioresins and biopolymers derived from natural resources as composites in drug delivery," in *Green Sustainable Process for Chemical and Environmental Engineering and Science*, Inamuddin and T. Altalhi, Eds., New York: Elsevier, 2023, pp. 21–34, doi: 10.1016/B978-0-323-95169-2.00007-9.

[17] B. Ates, S. Koytepe, A. Ulu, C. Gurses, and V. K. Thakur, "Chemistry, structures, and advanced applications of nanocomposites from biorenewable resources," *Chemical Reviews*, vol. 120, no. 17, pp. 9304–9362, Jul. 2020, doi: 10.1021/acs.chemrev.9b00553.

[18] C. Pavon, M. Aldas, J. Hernández-Fernández, and J. López-Martínez, "Comparative characterization of gum rosins for their use as sustainable additives in polymeric matrices," *Journal of Applied Polymer Science*, vol. 139, no. 9, Oct. 2022, Art. no. 51734, doi: 10.1002/app.51734.

[19] V. Limwibul, P. Jongvivatsakul, T. Jirawattanasomkul, J. G. Dai, and S. Likitlersuang, "Bioresin-based composites reinforced with natural fibers and carbon fiber: Mechanical properties and sustainable benefit assessment," *Journal of Materials Research and Technology*, vol. 36, pp. 140–156, Jun. 2025, doi: 10.1016/j.jmrt.2025.03.092.

[20] L. Ranakoti, M. Pokhriyal, and A. Kumar, "Natural fibers and biopolymers characterization: A future potential composite material," *Journal of Mechanical Engineering*, vol. 68, no. 1, pp. 33–50, 2018, doi: 10.1515/scjme-2018-0004.

[21] M. Dunky, "Applications and industrial implementations of naturally-based adhesives," in *Biobased Adhesives: Sources, Characteristics and Applications*, M. Dunky, K. L. Mittal, Eds., New Jersey: Wiley, Apr. 2023, pp. 659–704, doi: 10.1002/9781394175406.ch22.

[22] L. Deng, Z. Wang, B. Qu, Y. Liu, W. Qiu, and S. Qi, "A comparative study on the properties of rosin-based epoxy resins with different flexible chains," *Polymers*, vol. 15, no. 21, Oct. 2023, Art. no. 4246, doi: 10.3390/polym15214246.

[23] W. S. Lim, M. H. Kim, H. J. Park, and M. H. Lee, "Characterization of polyvinyl alcohol (PVA)/polyacrylic acid (PAA) composite film-forming solutions and resulting films as affected by beeswax content," *Polymers*, vol. 16, no. 3, Jan. 2024, Art. no. 310, doi: 10.3390/polym16030310.

[24] A. Lerma-Canto, M. D. Samper, I. Dominguez-Candela, D. Garcia-Garcia, and V. Fombuena, "Epoxidized and maleinized hemp oil to develop fully bio-based epoxy resin based on anhydride hardeners," *Polymers*, vol. 15, no. 6, Mar. 2023, Art. no. 1404, doi: 10.3390/polym15061404.

[25] B. Karacor and M. Ozcanli, "The use of bioresin composites created with five different vegetable oils such as soybean oil, palm oil, rapeseed oil, cottonseed oil, linseed oil in the automotive industry," *Polymer Composites*, vol. 46, no. 8, pp. 7091–7107, Dec. 2025, doi: 10.1002/pc.29415.

[26] A. S. Ismail, M. Jawaid, N. H. Hamid, R. Yahaya, A. Hassan, and S. N. Sarmin, "Physical, structural and thermal properties of bio-phenolic/epoxy polymers blends," *Materials Today Communications*, vol. 34, Mar. 2023, Art. no. 105455, doi: 10.1016/j.mtcomm.2023.105455.

[27] T. Anto, R. C.Rajendran, P. K. Muraleedharan, and E. Jayamani, "Effect of borax-boric acid treatment on fire resistance, thermal stability, acoustic, and mechanical properties of mycelium bio composites," *Applied Science and Engineering Progress*, vol. 17, no. 4, Oct. 2024, Art. no. 7271–7271, doi: 10.14416/j.asep.2023.11.007.

[28] A. N. Itua, O. I. Oluwole, D. O. Ojo, and A. M. Hope, "Abrasion resistance and water absorption characteristics of Ti-HAp hybrid reinforced polyetheretherketone biocomposites," *Applied Science and Engineering Progress*, vol. 16, no. 3, Sep. 2023, Art. no. 6728, doi: 10.14416/j.asep.2023.02.005.

[29] A. Sobhan, S. Saedi, M. Hoff, Y. Liang, and K. Muthukumarappan, "Evaluation and improvement of bio-based sustainable resin derived from formic-acid-modified epoxidized soybean oil for packaging applications," *Polymers*, vol. 15, no. 21, Oct. 2023, Art. no. 4255, doi: 10.3390/polym15214255.

[30] *Standard Test Method for Needle Penetration of Petroleum Waxes*, ASTM D1321–20, 2020.

[31] *Penetration of Fats and Oils (Needle Penetrometer Method*, AOAC official method 965.47, 1990.

[32] N. Deemoonmang, D. Tumnantong, B. Yoosuk, C. Ngamcharussrivichai, and P. Prasassarakich, "Preparation of wax esters from palmitic acid for superhydrophobic coating," *Journal of Industrial and Engineering Chemistry*, vol. 152, pp. 642–651, Dec. 2025, doi: 10.1016/j.jiec.2025.05.033.

[33] S. N. Syahida, Z. M. A. Ainun, M. R. Ismail-Fitry, and Z. A. Nur Hanani, "Development and characterisation of gelatine/palm wax/ lemongrass essential oil (GPL)-coated paper for active food packaging," *Packaging Technology and Science*, vol. 33, no. 10, pp. 417–431, Jun. 2020, doi: 10.1002/pts.2512.

[34] A. P. Osumah, "Synthesis and characterization of a biobased polymer from tung oil and pine rosin and characterization of polyhydroxybutyrate," Electronic theses and

dissertations, M.S. thesis, Department of Chemistry and Biochemistry, Georgia Southern University, 2025.

[35] D. Bhatia, C. Nimi, S. Sharma, A. K. Das, and R. Singh, "Rapid and non-destructive approach for characterization and differentiation of sealing wax using ATR-FTIR spectroscopy," *Journal of Forensic Sciences*, vol 68, no. 6, pp. 1982–1990, Aug. 2023, doi: 10.1111/1556-4029.15367.

[36] P. Samyn, C. Vanheusden, and P. Cosemans, "Performance of micronized biowax powders replacing PTFE fillers in bio-based epoxy resin coatings," *Coatings*, vol 15, no. 5, Apr. 2025, Art. no. 511, doi: 10.3390/coatings15050511.

[37] Y. Pan et al., "Characterization of epoxy composites reinforced with wax encapsulated microcrystalline cellulose," *Polymers*, vol. 8, no. 12, Nov. 2016, Art. no. 415, doi: 10.3390/polym8120415.

[38] J. Gomez-Caturla, J. Ivorra-Martinez, L. Quiles-Carrillo, M. P. Arrieta, and T. Boronat, "Terpenes: Nature's plasticizers for sustainable biopolymer enhancement," in *Sustainable Nanocomposites with Green Biomaterials. Biomaterials, Bioengineering and Sustainability*, R. Malviya, S. Sundram. Eds., Cham: Springer, 2025, vol. 2, pp 243–275, doi: 10.1007/978-3-031-79110-9_9.

[39] L. Yan, A. J. Huertas-Alonso, H. Liu, L. Dai, C. Si, and M. H. Sipponen, "Lignin polymerization: towards high-performance materials," *Chemical Society Reviews*, vol 54, pp. 6634–6651, Jun. 2025, doi: 10.1039/D4CS01044B.

[40] C. Farber, J. Li, E. Hager, R. Chemelewski, J. Mullet, A. Y. Rogachev, and D. Kurouski, "Complementarity of raman and infrared spectroscopy for structural characterization of plant epicuticular waxes," *Acs Omega*, vol. 4, no. 2, pp. 3700–3707, Feb. 2019, doi: 10.1021/acsomega.8b03675.

[41] N. R. Paluvai, S. Mohanty, and S. K. Nayak, "Studies on thermal degradation and flame retardant behavior of the sisal fiber reinforced unsaturated polyester toughened epoxy nanocomposites," *Journal of Applied Polymer Science*, vol. 132, no. 24, Feb. 2015, doi: 10.1002/app.42068.

[42] M. Khajouei, P. Pouresmaeel-Selakjani, and M. Latifi, "Spectroscopy and other miscellaneous techniques for the characterization of bio-epoxy polymers, their blends, and composites," in *Bio-Based Epoxy Polymers, Blends and Composites: Synthesis, Properties, Characterization and Applications*, J. Parameswaranpillai, S. Rangappa, S. Siengchin, S. Jose, Eds., New Jersey: Wiley-VCH GmbH, 2021, pp. 267–281, doi: 10.1002/9783527823604.ch9.

[43] L. Zhang and K. Song, "Study on the surface properties of hot-waxed wood with MCC filled fischer-tropsch synthetic wax," *Forests*, vol. 15, no. 12, Dec. 2024, Art. no. 2262, doi: 10.3390/f15122262.

[44] D. Gunwant, "Moisture resistance treatments of natural fiber-reinforced composites: A review," *Composite Interfaces*, vol. 31, no. 8, pp. 979–1047, Jan. 2024, doi: 10.1080/09276440.2024.2303543.

[45] R. Mori, "Replacing all petroleum-based chemical products with natural biomass-based chemical products: A tutorial review," *RSC Sustainability*, vol. 1, no. 2, pp. 179–212, Jan. 2023, doi: 10.1039/D2SU00014H.

[46] R. Dallaev, N. Papež, M. M. Allaham, and V. Holcman, "Biodegradable polymers: properties, applications, and environmental impact," *Polymers*, vol. 17, no. 14, Jul. 2025, Art. no. 1981, doi: 10.3390/polym17141981.

[47] A. Alhanish and M. Abu Ghalia, "Developments of biobased plasticizers for compostable polymers in the green packaging applications: A review," *Biotechnology Progress*, vol. 37, no. 6, Sep. 2021, Art. no. e3210, doi: 10.1002/btpr.3210.

[48] C. L. Esposito and P. Kirilov, "Preparation, characterization and evaluation of organogel-based lipstick formulations: Application in cosmetics," *Gels*, vol. 7, no. 3, Jul. 2021, Art. no. 97, doi: 10.3390/gels7030097.

[49] S. Pasieczna-Patkowska, M. Cichy, and J. Flieger, "Application of fourier transform infrared (FTIR) spectroscopy in characterization of green synthesized nanoparticles," *Molecules*, vol. 30, no. 3, Feb. 2025, Art. no. 684, doi: 10.3390/molecules30030684.

[50] P. Spencer, Y. Wang, J. L. Katz, and A. Misra, "Physicochemical interactions at the dentin/adhesive interface using FTIR chemical imaging," *Journal of Biomedical Optics*, vol. 10, no. 3, May 2025, Art. no. 031104, doi: 10.1117/1.1914844.

[51] M. S. Ganewatta et al., "Biobased plastics and elastomers from renewable rosin via "living"

ring-opening metathesis polymerization," *Macromolecules*, vol. 49, no. 19, pp. 7155–7164, Sep. 2016, doi: 10.1021/acs.macromol.6b01496.

[52] K. Z Hafila, R. Jumaidin, R. A. Ilyas, M. Z. Selamat, and F. A. M. Yusof, "Effect of palm wax on the mechanical, thermal, and moisture absorption properties of thermoplastic cassava starch composites," *International Journal of Biological Macromolecules*, vol. 194, pp. 851–860, Jan. 2022, doi: 10.1016/j.ijbiomac.2021.11.139.

[53] R. A. Sarria-Villa, J. A. Gallo-Corredor, and R. Benítez-Benítez, "Characterization and determination of the quality of rosins and turpentines extracted from *Pinus oocarpa* and *Pinus patula* resin," *Heliyon*, vol. 7, no. 8, Art. no. e07834, Aug. 2021, doi: 10.1016/j.heliyon.2021.e07834.

[54] M. L. Sanyang, S. M. Sapuan, M. Jawaid, M. R. Ishak, and J. Sahari, "Effect of plasticizer type and concentration on tensile, thermal and barrier properties of biodegradable films based on sugar palm (*Arenga pinnata*) starch," *Polymers*, vol. 7, no. 6, pp. 1106–1124, Jun. 2015, doi: 10.3390/polym7061106.

[55] F. Jahangiri, M. Amar, K. Akhilesh, C. Ryan, G. Stefano, and M. Manjusri, "Wax coatings for paper packaging applications: Study of the coating effect on surface, mechanical, and barrier properties," *ACS Environmental Au*, vol. 5, no. 2, pp. 165–182, Dec. 2024, doi: 10.1021/acsenvironau.4c00055.

[56] N. C. Saha, A. K. Ghosh, M. Garg, and S. D. Sadhu, "Flexible packaging material-Manufacturing processes and its application," in *Food Packaging*, Singapore: Springer, 2022, pp. 47–87, doi: 10.1007/978-981-16-4233-3_2.

[57] S. N. Danilova, A. V. Okoneshnikova, N. N. Lazareva, A. A. Okhlopkova, Z. F. Zhang, and B. F. Liu, "The role of wax origin in modifying ultra-high molecular weight polyethylene: Structure and properties," *Journal of Applied Polymer Science*, vol.142, no. 37, Jun. 2025, Art. no. e57460, doi: 10.1002/app.57460.

[58] M. J. Mochane, T. C. Mokhena, T. E. Motaung, and L. J. Linganiso, "Shape-stabilized phase change materials of polyolefin/wax blends and their composites."*Journal of Thermal Analysis and Calorimetry*, vol. 139, no. 5, pp. 2951–2963, Aug. 2020, doi: 10.1007/s10973-019-08734-3.

[59] B. Karacor and M. Ozcanli, "The use of bioresin composites created with five different vegetable oils such as soybean oil, palm oil, rapeseed oil, cottonseed oil, linseed oil in the automotive industry," *Polymer Composites*, vol 46, no. 8, pp. 7091–7107, Jun. 2025, doi: 10.1002/pc.29415.

[60] J. Yang, Y. C. Ching, and C. H. Chuah, "Applications of lignocellulosic fibers and lignin in bioplastics: A review," *Polymers*, vol 11, no. 5, Apr. 2019, Art. no. 751, doi: 10.3390/polym11050751.

[61] M. M. Nobrega, J. B. Olivato, C. M. O. Müller, and F. Yamashita, "Addition of saturated fatty acids to biodegradable films: Effect on the crystallinity and viscoelastic characteristics," *Journal of Polymers and the Environment*, vol. 21, pp. 166–171, May 2013, doi: 10.1007/s10924-012-0477-7.